Computers and Chemical Engineering 166 (2022) 107971

Contents lists available at ScienceDirect

Computers and Chemical Engineering

journal homepage: www.elsevier.com/locate/compchemeng

Heat transfer in pipes with twisted tapes: CFD simulations and validation

Rubén Cabello *, Alexandra Elena Plesu Popescu, Jordi Bonet-Ruiz, David Curcó Cantarell, Joan Llorens

Department of Chemical Engineering and Analytical Chemistry, Faculty of Chemistry, University of Barcelona, c/ Martí i Franquès 1, 6th Floor, Barcelona 08028, Spain

A B S T R A C T

Inserts are placed inside heat exchangers to promote turbulence and maximize the heat transferred. Twisted tapes enhance heat transfer with minimal pressure drop increase for double pipe heat exchangers. Their design typically relied on experimental correlations, but nowadays CFD software is gaining interest. The choice of the turbulent model is of paramount importance and not addressed in the literature. This research aims to compare the combinations of k-ε, k-ω and RSM as well as their different wall treatments available in Ansys Fluent® and literature experimental data. Different twist ratios and Reynolds numbers are tested. Currently, no research is found in literature comparing different CFD methods for this type of units. The main objective of this research is to find the combination of RANS turbulent model and wall treatment that will most accurately reproduce the global values needed (Nusselt number and friction factor) when designing a heat exchanger with twisted tape inserts. Results show that the selection of the wall treatment is far more relevant than the turbulence model. Simulations have less discrepancy between themselves than the empirical correlations. Best performing models were k-ε Standard with ML wall treatment, which provided an average deviation from correlations ranging between 15 and 18%. K-ω SST models also provided accurate performance when estimating friction factor values with 17 to 20% deviation. Results provide clues for choosing a suitable turbulent model and are useful to minimize the error provided by the models.

1. Introduction

In recent years with the impending oil shortage and other non-renewable resources, energy efficiency has become a worldwide concern from economic and environmental points of view. Modern industries have to adapt their processes and equipment if they want to compete in global market. Heat transfer mechanisms are present in most of chemical industries and are critical for improving their energy efficiency and consumption. The improvement of the heat exchanger network of existing plants often becomes constrained by the place available for larger heat exchangers. Rather than using active heat transfer enhancement methods, which require input of external power often leading to complex modifications and poor efficiency improvement, most companies opt for passive heat transfer mechanisms. These methods include the use of swirl producing devices and the modification of the tube geometrics, which are fairly simple modifications that allow heat transfer improvement by improving the turbulence of the fluid and the contact area. In most cases, a numerical study is conducted previous to the modifications to optimize the geometric parameters, which can be conducted with CFD simulations.

The experimental research done in this topic has been extensive, testing all sorts of twisted tape (TT) shapes alongside other geometrical combinations. Nusselt number (Nu) and TPF (Thermal Performance Factor) are the two major variables that are to be optimised, as the first is directly related to the amount of heat transferred and the second describes the energetical efficiency of the process in terms of heat transfer and pressure drop. A closer look into experimental studies is provided. Research performed by Liao and Xin (2000) combined the use of TT with extended 3D surfaces inside the tubing, finding improvement with respect with plain tubes. This improvement, however, is only relevant outside the turbulent regime, for highly viscous fluids. Chang et al. (2007) correlated pressure drop and Nusselt number. Eiamsa-ard et al. (2009) tested twisted tapes of different length with plain tubes. They found up to 15.3% increase in heat transfer when full length twisted tapes were used. Later, Eiamsa-ard et al. (2010) compared the effects of single and dual twisted tapes (two parallel twisted tapes). While doing so, very useful correlations were also provided for twisted tapes in the range of study. TT inserts increase from 36% to 48% the heat transferred due to the centrifugal forces induced by the spiral motion in the fluid (Naga Sarada et al., 2012).

Some experimental studies combine TT with other sorts of inserts. Hasanpour et al. (2016) analysed the combination of helical corrugated tubes and perforated TT and concluded that the combination of TT and corrugated tubes increased the Nu more than corrugated tubes alone. Chu et al. (2020) studied different v-cut TT shapes at the turbulent transition zone. The results obtained shows TPF of 1.18–1.23 for the obtuse v-cut TT which is the one that gave better results. Wang et al. (2020) compared the use of TT and HC (Helical Coils) and the presence of both inserts at the same time. It was found that HC alone improved

* Corresponding author.
E-mail address: ruben.cabello@ub.edu (R. Cabello).

https://doi.org/10.1016/j.compchemeng.2022.107971
Received 3 March 2022; Received in revised form 22 August 2022; Accepted 27 August 2022
Available online 28 August 2022

Nomenclature

μ_t	turbulent viscosity (kg (m s)$^{-1}$)
BSL	menter baseline model
CFD	computational fluid dynamics
d	tape width (mm)
D	tube diameter (mm)
EWT	enhanced wall treatment
f	friction factor (dimensionless)
HC	helical coil
l	TT length (m)
K-ε	K-epsilon turbulent model
K-ω	K-omega turbulent model
L	tube length (m)
Low-Re	Low-Reynolds corrections
ML	Menther-Lechner
NEWF	non-equilibrium wall functions
Nu	Nusselt number (dimensionless)
NWM	near-wall modelling
Quad.-	quadratic
Re	Reynolds number (dimensionless)
Real.	realizable
RNG	Re-Normalisation Group
RSM	Reynolds Stress Models
SST	shear stress transport
St.	standard
SWF	scalable wall functions
T_i	inlet temperature (K)
TPF	thermal performance factor (dimensionless)
TR	twist ratio (dimensionless)
TT	twisted tape
T_w	outer wall temperature (K)
v_i	inlet velocity (m/s)
y	tape pitch length (mm)

heat transfer more than TT but resulted in a substantial increase in pressure drop. The resulting TPF was highest when both TT and HC were together, followed by the use of TT and HC, which produced overly high pressure drop for the heat enhancement yielded. There is an interest in studying complex configurations, as they increase Nu and TPF.

More experimental research is being developed constantly, but CFD models are more and more frequently used in this field of research, often alongside experimental data. They offer tools to model these units efficiently and bring the opportunity of reducing experimental costs by finding optimal values for the geometrical and the input parameters of the heat exchangers. Shabanian et al. (2011) used CFD modelling to predict turbulence effects and explain experimental observations in an air cooler equipped with different tube inserts. The difference between experimental and CFD results ranged from 3.5% to 7.3% for Nusselt number and friction factor. The amount of passive heat enhancement methods related research that is developed with CFD should be enough proof to label them as viable for these studies. Natarajan et al. (2020) studied both experimentally and with CFD the effect of enhancement in heat transfer that the combination of different twisted tapes with different twist ratios and a working fluid composed of water and SiC nanoparticles. Both horizontal wings twisted tapes and plain twisted tapes were used for this work with the first giving more promising results. The error difference between the CFD study and the experimental case was between 5% and 9% for Nusselt number and friction factor. Sharma and Kumar Patel (2020) studied different twist ratios and different Reynolds numbers in a counter flow heat exchanger. One twisted tape had alternating clockwise and counter-clockwise twists while the other had semi-circular notches every two twists. In this research, the RANS model that fits the best this kind of simulation is RSM (Reynolds Stress model) and proved that CFD is in close agreement with experimental studies.

CFD models are often used for optimising geometries like the work developed by Noorbakhsh et al. (2020) who explored the effects of enhancement when both tubes (internal and external) are suited with twisted tapes. Hollows were also created with different aspect ratios (AR=W/H) in the twisted tapes. The results show that creating the hollows with AR = 1 on the twisted tape leads to higher coefficient of performance. He et al. (2020) considered the effect of adding an additional TT insert and compared it to the use of a unique TT. CuO-water nanofluid at different concentrations was also used. The results proved that the use of two TT increased the Nu significantly more than the sole TT but the pressure drop masks the heat transfer enhancement yielding Thermal Performance Factor (TPF) values under those found with single TT. Nakhchi and Esfahani (2020) performed a CFD analysis of CuO nanofluid flowing on tubes with louvered strip inserts, proving that TPF could raise to 1.99 when the angle of the strips is 25° and there are perforations on each of them. Tiwari et al. (2021) analysed the thermal performance of a triple tube heat exchanger both experimentally and with CFD. The fluid used was WO_3/ Water nanofluid and there were inserts inside the middle tube. In this case, rib inserts performed better than porous or TT inserts, although all of them showed improvement with respect to a plain tube. Zaboli et al. (2022) studied the combination of a corrugate coil tube with a spiral twisted tape. Five lobe corrugated tubes showed the best thermal performance, with an improvement of Nu of 30.7% and an increase in pressure drop of 37.1%. The TPF for these configurations was found to be 1.20–1.21. CFD models are even used to create correlations, which can mitigate the major downside of CFD: the computational time and cost that some cases require.

CFD tools are currently used for optimizing or providing correlations. Pourfattah et al. (2021) combined two powerful computational tools: Genetic Algorithms and CFD. In this way, the optimization of a twisted tape heat exchanger with five design points was achieved and found a 265% increase in heat transfer with respect to the plain tube. Oni (2021) used Ansys Fluent® to simulate different twisted tape shapes and inserts, finding correlations for the friction factor (f) and the Nusselt number (Nu) with Reynolds number, Prandtl number, tape's width, tape's pitch, and tape's perimeter of opening. Amongst the shapes studied, tapes with intersected axes and triangle-shaped openings were found to give best results for laminar flow.

The cases mentioned previously often lack realistic comparison between CFD results and experimental data or between different turbulent models and/or wall treatment methods. When it comes to choosing a turbulent model, most authors rely on previous studies with similar conditions. Sometimes it is just assumed that if for a geometry and settings a turbulent method predicts results accurately, it must be reliable for any other case. Scarce sources are found in which research is performed to compare different turbulent models and often the exact model or the wall treatment used is omitted. This study is focused on testing how reliable different turbulent models and wall treatments are when studying twisted tapes inserts. Different turbulent models are compared against correlations extracted from experimental data on twisted tapes. Different geometries and Reynolds numbers are tested to prove whether the accuracy of these models has a dependency of the case studied, and if so, which is the best model for every situation.

2. Methodology

In order to test consistently different models and wall treatments, every other source of error has to be reduced to the minimum possible values. According to Ansys Fluent (Oswald, 2015) there are five sources

of error: Round-off, iteration, discretization, model and systematic. Round-off errors are produced when the numerical precision of the computer is not enough. In order to avoid this kind of errors, all CFD simulations in this project are performed with double precision variables. Iteration errors occur when solutions are not fully converged, or the solution oscillates between values. This error is often mitigated with sufficient iterations to ensure convergence. In some cases, the model or the mesh can cause numerical instability which can affect the convergence. Discretization errors occur when the mesh is not fine or has not enough quality, often misrepresenting the geometry or not allowing sufficient representation of the gradients present in the problem. While tetrahedrons meshes can cover extreme geometries, they often come with errors such as numerical diffusion. Prism meshes on the other hand, usually avoid this type of errors, and are used in this research for all the models. Mesh optimization is key to avoid these errors. The model error is what this research seeks for. Different models can lead to different results, as their formulation and constants differ from one to another. Most models require specific conditions to operate optimally. That is, models such as k-ω require that the first node located at a fluid region is at a distance $y+\approx 1$. Wall function methods often ask for a coarser mesh, requiring meshes at a $y+>30$ to give proper results. When using wall functions, this research will focus on wall functions insensitive to $y+$. Different meshes are designed according to the different requirements of each model. For k-ε, the mesh is optimised according only to the cell size, as all of the wall treatments used are said to be $y+$ insensitive. For k-ω models, the cell size is optimised and then a mesh adaptation is performed to ensure that all the nodes in the domain have at least $y+\approx 1$ at the first node near the wall (ANSYS Fluent Theory Guide, 2021). Fig. 1 illustrates the steps followed for this problem solving. First, geometrical design of the twisted tapes is performed, then the mesh is generated and optimized for each model via a mesh independency study. The setup is performed to match similar conditions as those found in the semi-empirical correlations and then the numerical resolution is carried out alongside a dynamic mesh adaptation to ensure $y+\approx 1$ for the omega models. Results are compared with correlations using different methods and conclusions are extracted.

2.1. Problem description and geometry

Simulations are conducted so that they emulate the conditions present in Eiamsa-ard et al. (2010) experimental procedures. The setup consists of a single tube with a twisted tape insert and surrounded by an electrical heater. For emulating the electrical heater, temperature will be assumed to be constant at the outer wall of the pipe. Different twist ratios (TR, defined as y/d) and Reynolds numbers are tested. Fig. 2 describes the different variables in the domain.

Here, the input variables are the inlet temperature T_i; the wall temperature T_w; the inlet velocity v_i, the outlet pressure P, which is set to atmospheric pressure; and the different geometrical parameters. As for the output parameters, P_i is set to be the pressure at the inlet, which is compared against P_o, the pressure at the end of the TT, which is the relevant section of the simulation. Temperature T_o is also taken at the end of the TT. The reasoning behind the twisted tape not covering the full length of the pipe is that pressure outlets near obstacles can produce backflow errors, leading to poor convergence. By extending the pipe, it is guaranteed that the flow at the outlet flows in the same direction, avoiding the mentioned issue. The average pressure and temperature are also monitored in various lengths along the tube to test whether the profiles have stabilized and if the entrance effects are relevant in this scheme. If these effects are large enough, the comparative values of pressure and temperature are then taken from a point where the profile is already stable. Table 1 describes the different input parameters of the system, similar to those found in Eiamsa-ard et al. (2010).

The working fluid is air, whose properties such as thermal conductivity (k), specific heat (cp) and viscosity (μ) are temperature dependant. Ideal gas model is selected for this case, as air is compressible.

2.2. Experimental correlations used

Several correlations that proceed from experimental results are found in the literature. It is often the case that the range for which those correlations are designed does not match exactly the range of the simulations performed. Eqs. (1) and (2) are found in Eiamsa-ard et al. (2010), valid for all the range of simulations.

$$Nu = 0.06\ Re^{0.75} Pr^{0.4}\ TR^{\ -0.26} \tag{1}$$

$$f = 10.02\ Re^{-0.46}\ TR^{\ -0.48} \tag{2}$$

where Re is the Reynolds number, Pr is the Prandtl number and TR is the twist ratio. Other correlations are found in Chang et al. (2007), where the range of TR goes from 1.56 to 2.81. Their results should be at least suitable for our simulations with TR =3, as for higher twist ratios the extrapolation of the equations could lead to errors. Functions generated by Manglik et al. (1992) are employed to estimate Nusselt numbers. Date (1974) also found correlations for laminar and turbulent flows with a range of $Re/Tr \geq 100$ also valid in this research, useful for estimating friction factors. The previously mentioned studies are widely used and accepted, being also validated by other studies such as Kumar and Prasad (2000).

2.3. Turbulent models

In this section the turbulent models and wall treatments are classified without entering in much detail of the equations used by all the models. From the turbulent models available, this research is focused on RANS (Reynolds Averaged Navier-Stokes) models, more specifically in two-equation Eddy viscosity models and Reynolds Stress Models (RSM). LES (Large Eddy Simulations) and other similar models which require Subgrid-Scale turbulent models are discarded due to the high computational costs and time that they require as well as the long flowtime required to obtain reliable engineering values. Two-equation Eddy viscosity models and RSM are the ones that are currently most used for modelling these units, as they offer a fair trade between accuracy and computational requirements. They are time-averaged, which means the variables extracted from the models can be of engineering interest, as they are not time-dependant. Two of the most relevant RANS models nowadays are k-ε and k-ω based models and their variants. The main difference between them lays in how those models behave in free shear flow situations and wall bounded ones. K-ε models are more reliable away from boundaries, where free shear flows are present. As such, they require additional equations for modelling the domain close to boundaries, that may come in form of wall functions or additional models. As a

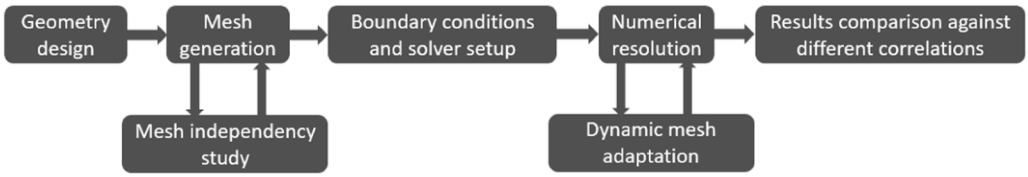

Fig. 1. Problem solving steps scheme.

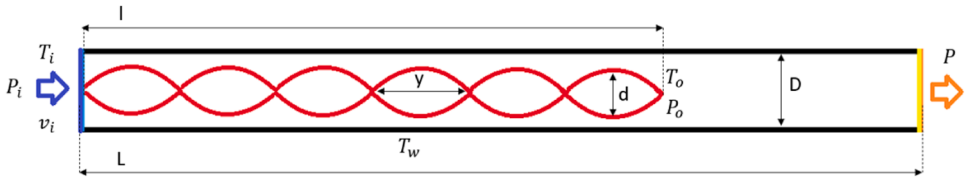

Fig. 2. Outline of the problem with its domain variables. In blue is depicted the velocity inlet and in orange the pressure outlet.

Table 1
Values for different variables.

Parameter	Value(s)
Inlet velocity (v_i)	4, 6, 8, 10, 12 m/s
Inlet temperature (T_i)	300 K
Reynolds number (Re)	From 4 000 to 19 000
Tube length (L)	1.75 m
TT length (l)	1.25 m
Tape pitch length (y)	138, 184, 230 mm
Twist ratio (TR= y/d)	3, 4, 5
Tube diameter (D)	47 mm
Tape width (d)	46 mm
Tape thickness	0.8 mm
Outer wall temperature (T_w)	363 K

counterpart, k-ω is a low Reynolds model, which means that is better suited for wall bounded flows, decreasing in accuracy for free-shear flows. These reasons lead to models like k-ω SST to be a combination of k-ω and k-ε each applied at the region where they are more accurate by using a blending function. RSM models require more computational time, but unlike two-equation models, they do not rely on the Boussinesq approach which assumes that the turbulent viscosity (μ_t) is isotropic (Hinze, 1975). Seven additional transport equations are required by RSM to compute μ_t which create anisotropy in the turbulence. In cases with swirling flows such as this one RSM can yield better results as two-equation models. Further details about the models and its equations are available in ANSYS Fluent Theory Guide (2021).

Table 2 shows each turbulent model variant combined with each wall treatment, generating a total of 19 combinations tested in the present study. For k-ε models (both k-ε and k-ε based RSM) wall functions are implemented as well as wall modelling methods such as Enhanced Wall Treatment (EWT) and Menther-Lechner (ML), all of which are $y+$ insensitive. EWT treatment is selected with the additional option of pressure gradient effects and thermal, which would consider the presence of large pressure or temperature gradients near the walls if there were any. K-ω based models are all suited with free shear flow improvements by using blending functions with k-ε (SST and Stress BSL) or the shear flow corrections of the Stress Omega model.

Table 2
Different models and wall treatments.

Turbulent model	Variants		Wall treatments
K-ε	Standard RNG Realizable		Scalable Wall Functions (SWF) Non-equilibrium wall functions (NEWF) Enhanced Wall Treatment (EWT) Menther-Lechner (ML)
K-ω	SST		Default k-ω modelling Low-Reynolds corrections
RSM	K-ε based	Linear Pressure Strain Quadratic Pressure Strain	Scalable Wall Functions (SWF) Non-equilibrium wall functions (NEWF) Enhanced Wall Treatment* (EWT)
	K-ω based	Stress Omega ** Stress BSL	Default k-ω modelling

* Only available for Linear Pressure Strain.
** With shear flow corrections.

2.4. Mesh optimization

The mesh optimization is different for k-ε based models and for k-ω based models. For k-ε models, the relevant mesh optimization is performed only for the cell size, as all of the wall treatments are insensitive to $y+$. Inflation layers are also tested with these models and the results show that the influence on the final results of decreasing $y+$ is minimal. Different node distance values are tested, and the most relevant variables are then extracted: pressure drop and temperature.

2.5. Convergence

To ensure convergence it is not sufficient to track residuals, which are dependant on how close from the solution are the initialization values. Two additional variables are tracked: area-weighted average pressure at the inlet and area-weighted average temperature at the outlet. These are relevant variables which have to be converged in order to validate the results. All residuals in the simulations are converged to at least 10^{-5}, as same as for the tracked variables for 30 iterations. For most models though, the convergence criteria is much more strict, making almost all the simulations converge to 10^{-7} for residuals and tracked variables, as seen in Fig. 3.

3. Results and discussion

3.1. Mesh independency results

Mesh independency tests are performed to find the optimum values of mesh size used in the simulations. Fig. 4 shows the pressure drop results for different models and wall treatments at the same conditions.

As shown, for k-epsilon models results become stable when the grid size is small. At sizes of 0.001 m, it can be considered that results are precise enough. For k-omega based models is quite the opposite, having an increasing tendency as the size decreases. This effect is produced by the near wall, modelling of these models and is mitigated once the mesh adaptation ensures that near the wall the first node is at a distance $y+<1$ from the wall, as with the same conditions and mesh adaptation the results are similar to the extrapolation of each model when mesh size approaches 0.

The final selected mesh is a polyhedral mesh with a cell size of 0.001 m. The total number of nodes is around 27 M. For k-ω based models, additional mesh adaptation is performed to ensure $y+<1$ at the boundaries. This adaptation results in meshes of about 70 M nodes. The minimum orthogonal quality is kept above 0.2 and the maximum skewness under 0.9. Fig. 5 shows the resulting polyhedral mesh, where smaller cells are present near the gaps between the pipe and the twisted tape.

3.2. Correlation's deviation

In this section, literature correlation equations for twisted tape inserts are compared. The correlations in this research do not always yield

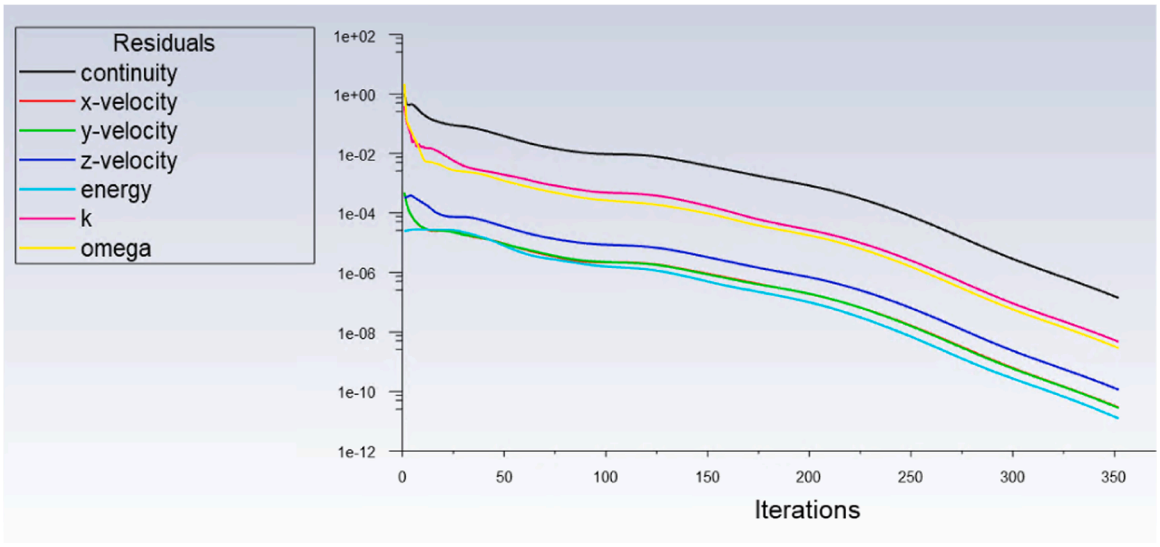

Fig. 3. Example of convergence in a k-omega model.

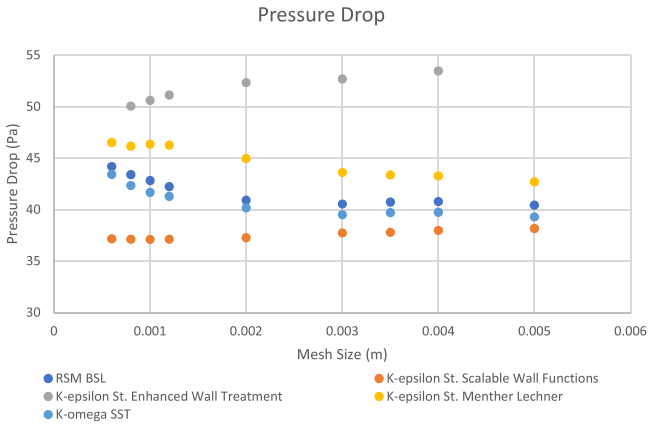

Fig. 4. Mesh independency results.

similar results. Those correlations are performed in different experimental conditions, such as Reynolds number and working fluid, so their results differ significantly from one to another. Depending on Reynolds number and TR, there are also variations amongst correlations of up to 56% for friction factor at low Reynolds numbers and up to 48% for Nusselt number. Correlations by Date (1974) and Eiamsa-ard et al. (2010) prove to be more consistent between them, as the deviation between them is low in most of the cases. Chang et al. (2007) correlations' have proven to have more deviation for this case as there are designed for lower TR than the ones presented. Turbulent models that can provide results close to the ones found in the first two correlations are regarded in the present work as better and more accurate. Fig. 6 shows that correlations prove to be more consistent with each other as twist ratio increases. It can also be observed that Nusselt number deviation between correlations increases with Reynolds, whereas friction factor decreases.

3.3. Stabilization profile results

Profile stabilization is a key element when comparing against correlations, as they assume fully developed profiles. To ensure that the results are in a fully developed form, only the parts of the pipe where the pressure and temperature profiles are linear are considered.

Values between 0.75 m and 1.25 m from the inlet are considered as the profile in this region becomes linear. For some models profile stabilization occurs more rapidly than others, but from the 0.75 m mark, all do present a linear profile. Fig. 7 shows that the profile starts to become

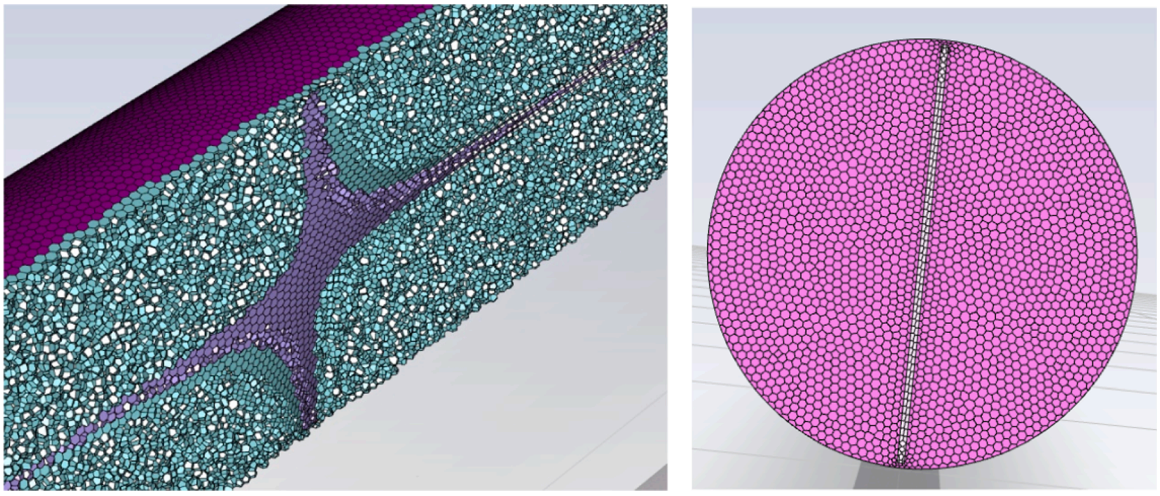

Fig. 5. Mesh results (a) side view of the twisted tape, (b) Mesh at the inlet face.

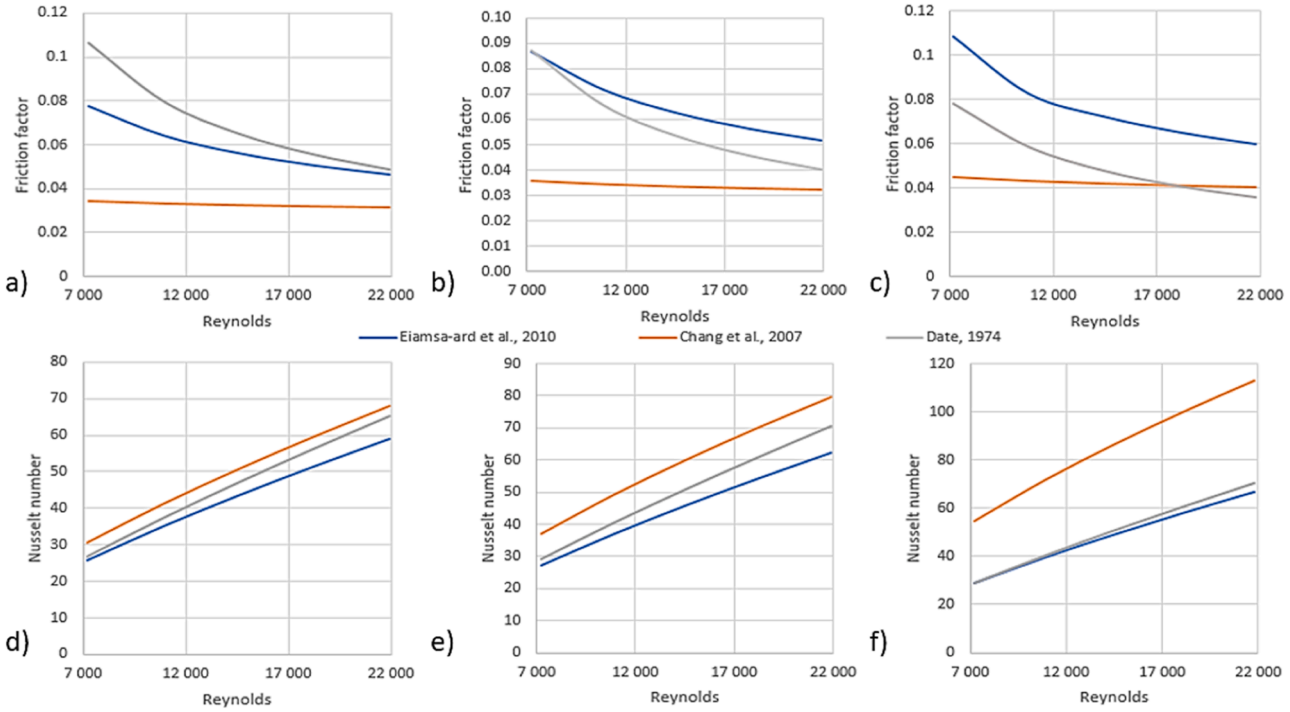

Fig. 6. Correlations comparison (a) Friction factor from different correlations TR=5 (b) Friction factor from different correlations TR=4, (c) Friction factor from different correlations TR=3, (d) Nusselt number from different correlations TR=5, (e) Nusselt number TR=4 (f) Nusselt number TR=3.

linear and stabilized at a distance 0.7 m from the inlet. The points where $P = 0$ correspond to the presence of the twisted tape, that since it is a solid, the program takes its pressure as 0. Values such as velocity and temperature follow a similar trend but are too chaotic in the presence of a twisted tape to display them. Instead, the profile perpendicular to the motion of the fluid is displayed.

Fig. 8 illustrates that temperature profiles develop early in the tube, as for lengths of 0.62 m from the inlet, the profile is fairly stabilized. It is observed that the profile is unstable at $l = 0.14$m, presenting a disruptive change in temperature at around 0.016 m of the centre. Despite this, values are again taken from the 0.75 m mark. This graph also shows which reference will be used for estimating the Nusselt number: $T_\infty = 322$K in this case. T_∞ is estimated as the average bulk temperature in the middle of the interest zone: at 1 m from the inlet.

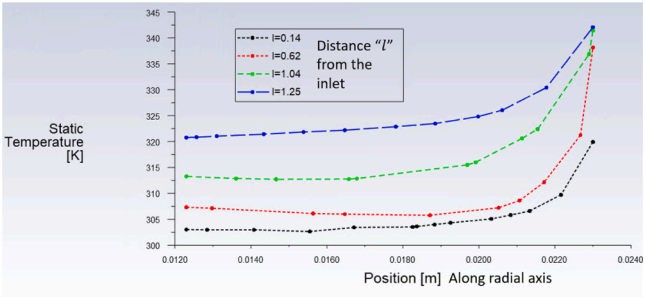

Fig. 8. Temperature profiles at different distances "*l*" from the inlet with respect to the radial position. TR=3, *Re*=10,000. Model: K-ε RNG SWF.

3.4. Turbulent model results

This section is divided in order to cover every model and wall treatment. Some models are showcased in Figs. 9–12.

The Figs. 9–12 show that all models may be suitable for the simulation of the heat exchanger, as their expected deviation will be similar to the ones found between correlations themselves. Figs. 9–11 show how even at different TR values the different wall treatments of the k-ε standard model each follow a different experimental correlation. For

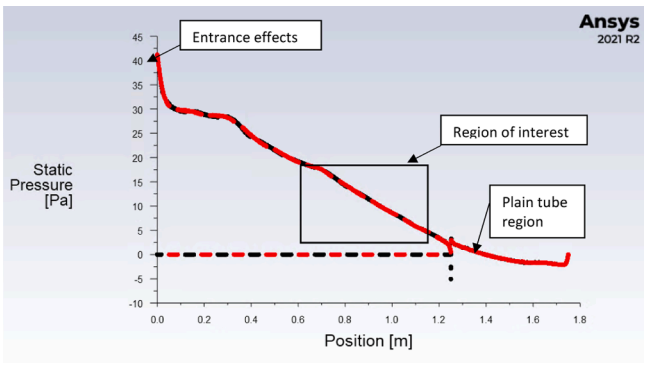

Fig. 7. Pressure profile along two lines parallel to the twisted tape (one in red and the other in black). TR=3, *Re*=10 000. Model: K-ε RNG SWF.

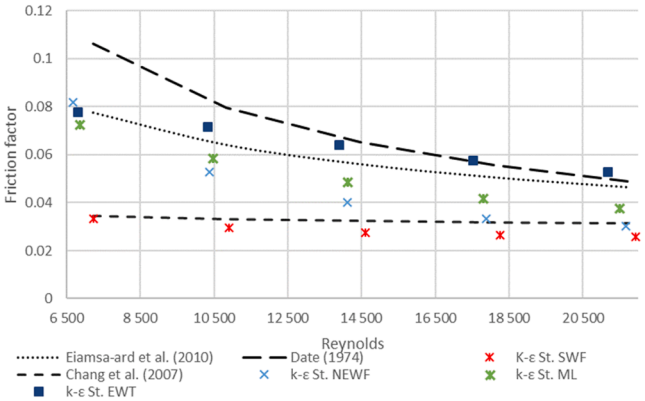

Fig. 9. Friction factor for some turbulent models (TR=5).

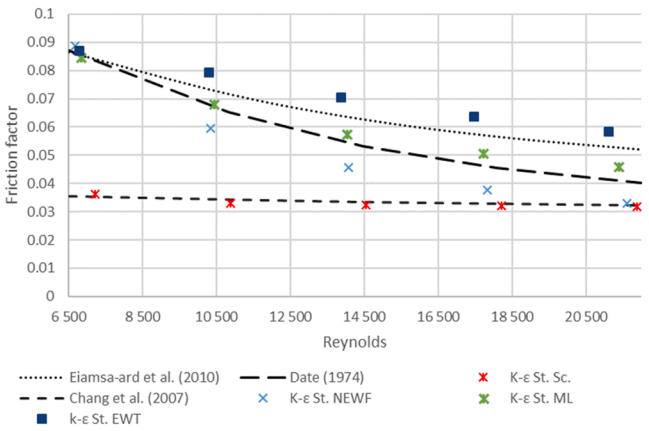

Fig. 10. Friction factor for some turbulent models (TR=4).

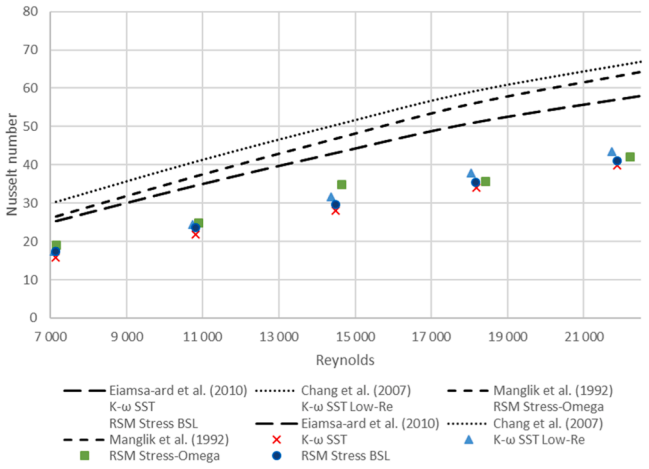

Fig. 11. Nusselt number CFD vs Correlations for K-ω based models (TR=5).

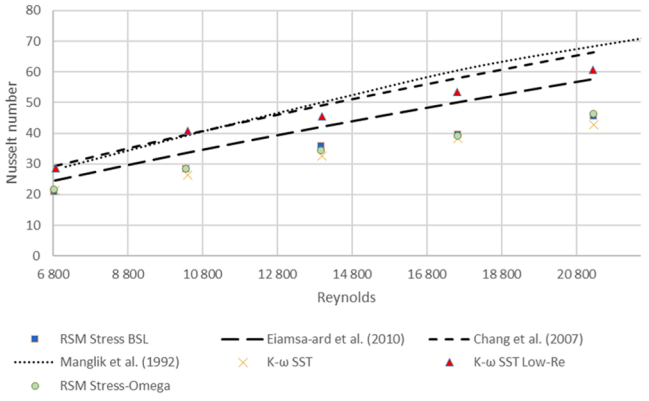

Fig. 12. Nusselt number CFD vs Correlations for K-ω based models (TR=3).

Figs. 11 and 12 it can be seen that k-ω based models are less accurate at high TR, but for a lower TR they yield values close to those of the empirical correlations. In order to decide which model better performed for this scenario, results are compared against the correlation found in Eiamsa-ard et al. (2010) as it is the one which was obtained with the same domain variables as the simulations performed in this work. These results do not mean that turbulent models with high deviation are not accurate as they most probably follow the trend of another correlation, as seen in Figs. 11–13 where RSM Quadratic Scalable and K-ε Standard wt. Scalable Wall Functions followed correlations found in Chang et al. (2007), while other models lean towards the results found in Eiamsa-ard et al. (2010).

The deviation between each turbulent model and the correlations described has a dependency on the geometry variables (in this case different TR) and the Reynolds number. A grid is generated testing all the combinations along the 5 different Reynolds numbers in that range from 7 000 to 21 000 and the 3 TR. In order to study how the TR affects the deviation of each model with respect to experimental correlations, the deviation value is averaged along all simulations with the same TR. Later, the deviation present in all simulations' results with the same Reynolds is averaged, in order to study the total deviation produced by different Reynolds numbers.

Table 3 shows the discrepancy or deviation between simulation results and those found using Eqs. (1) and (2). The combination that gives a better performance is k-ε Realizable ML, which in average has the lowest deviation. The total average shows the expected deviation if a turbulent model and wall treatment is chosen randomly, showing how good the performance of these models are in average.

Clear relationships can be derived from the data collected. For k-ε models there is much more influence on the final results of the wall treatment used than the specific turbulent model selected. The wall treatments that better adjust the experimental correlations are Menther-Lechner and Enhanced Wall Treatment, both being designed to avoid the ideal assumptions present in wall functions. Menther-Lechner treatment is advised when dealing with complex geometries such as this case. Simple models such as SWF prove to be inaccurate for this complex geometry, they underestimate friction factors and Nusselt number, which can lead to huge errors when calculating TFP. If wall functions are to be used, non- equilibrium wall functions are better suited for complex flows. When estimating Nusselt number, which is the major design interest in these problems, k-ω models prove to yield accurate and consistent results.

In Figs. 13 and 14, the different values of friction factor (f) and Nusselt number (Nu) are compared to those obtained from Eiamsa-ard et al. (2010)'s equations. K-ε models and k-ω based models, seem to give similar results between themselves, both for f and Nu. K-ω based models have a low dependency on Low-*Re* treatment or if the RSM is selected.

In general, all models present a mean bias with respect to Eiamsa-ard et al. (2010)'s correlations that makes the consistently underestimate pressure drop by about 22%. In the case of Nu, they underestimate it by a 3% in average. Lowest bias was found in k-ε standard EWT for friction factor and k-Ɛ Realizable NEWF, the later being accurate but not precise enough.

Fig. 15 presents the mean deviation with respect to Eqs. (1) and (2) of each combination of model and wall treatment. There are combinations that work much better than others. K-ω based models gave good results, with k-ω SST Low-*Re* giving better results than the others. In general, RSM models did not give a better accuracy in validating experimental data. For k-ε based models, all of the models which include EWT or ML produced accurate and precise friction factors and Nusselt numbers. There seems to be little to no influence on how the combination of turbulent models and wall treatments affect the results, as the outputs seem to be the sum of the two influences independently.

All of the above conclusions are extracted solely by comparing the simulation results with the experimental correlations extracted from the same unit. Different conclusions can be extracted if results are compared with the average value of the three correlations reviewed. Chang et al. (2007) results are only considered in the TR=3 case, as in their experimental procedures the TR ranged from 1.56 to 2.81, not covering our region of interest. Total deviation is calculated as shown on Eq. (3):

$$dv = Abs\left(\frac{a_s}{\sum w_i a_{ci} / \sum w_i} - 1\right) \tag{3}$$

Where a_s is a simulation variable result, a_{ci} is the same variable extracted from the "ith" correlation and w_i is the weight or importance

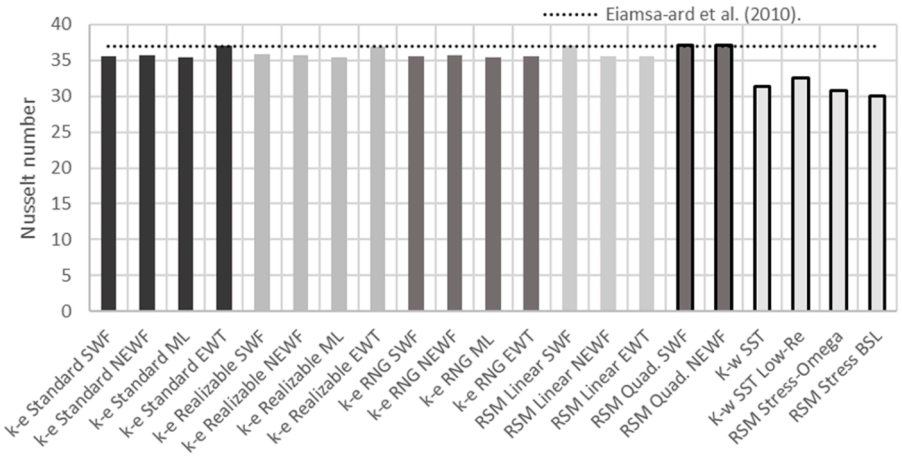

Fig. 13. Nusselt number comparison between different models (TR=4, *Re*=10 000).

Table 3
Averaged deviation of the different turbulent models at different twist ratios.

	TR=3		TR=4		TR=5	
	f deviation (%)	Nu deviation (%)	f deviation (%)	Nu deviation (%)	f deviation (%)	Nu deviation (%)
k-ε Standard SWF	44.73	38.80	48.56	41.63	50.84	48.27
k-ε Standard NEWF	21.29	25.14	23.64	27.13	24.37	30.66
k-ε Standard ML	5.61	22.66	9.11	20.73	14.62	16.85
k-ε Standard EWT	12.80	26.25	8.33	20.35	9.11	22.65
k-ε Realizable SWF	47.10	42.35	51.43	45.41	53.72	52.06
k-ε Realizable NEWF	24.63	21.00	29.36	23.45	30.67	25.61
k-ε Realizable ML	4.73	23.33	8.73	20.97	14.20	16.91
k-ε Realizable EWT	14.02	29.93	8.60	22.29	9.65	25.08
k-ε RNG SWF	45.39	39.58	49.08	41.67	51.07	47.74
k-ε RNG NEWF	21.34	29.23	24.89	27.59	25.86	32.45
k-ε RNG ML	6.68	23.03	9.42	20.76	14.91	16.77
k-ε RNG EWT	14.55	34.27	8.30	24.57	8.90	27.18
RSM Linear SWF	47.16	42.77	11.35	18.09	55.26	53.60
RSM Linear NEWF	24.72	30.21	51.55	44.66	33.34	32.93
RSM Linear EWT	18.11	32.01	29.92	27.52	9.08	15.23
RSM Quad. SWF	47.11	42.45	30.65	28.09	55.42	53.90
RSM Quad. NEWF	25.40	30.21	52.04	45.61	33.97	32.42
K-ω SST	22.24	21.42	15.55	7.19	48.74	35.18
K-ω SST Low-*Re*	19.73	11.46	13.40	21.82	40.65	27.69
RSM Stress-Omega	20.31	17.49	17.50	24.67	64.12	46.34
RSM Stress BSL	23.40	20.98	17.61	26.71	52.36	30.97
Average Total	24.34	28.79	24.71	27.66	33.37	32.88

that is assigned to the correlation, in this case $w_i = 1$ for all the cases except for Chang et al. (2007)'s correlations in cases TR=4 and TR=5, where $w_i = 0$. By using this equation, the first comparison has $w_i = 1$ for Eiamsa-ard et al. (2010)'s correlations and $w_i = 0$ for the others.

The results of using the second comparison method are displayed in Table 4, where values are compared against the mean correlation value and their deviation is averaged for the different Reynolds numbers.Here the method that shows less discrepancy with experimental is the k-ω SST. Models that did not have high accuracy in the first method do not present it here either, like the case of SWF. Fig. 16 illustrates the different average deviation from the mean experimental value for the models studied. It is noticeable how in this case the method with lower friction factor deviation is the k- ω SST.

It is hard to decide which correlation is more reliable, which propagates to turbulent models and wall treatments. Most combinations of models and wall treatments provided similar deviations for both comparisons. The mean deviation result of the two comparative methods can be used, which is analogous to giving twice the weight when averaging to Eiamsa-ard et al. (2010)'s equations. In fact, during the averaging process, the weights can be adjusted to the needs or beliefs of the user on which correlation is better suited for the parameters of the domain. This research presents the two extreme cases: either the user considers all correlations equally, or only considers one is correct. Each other case falls between those two cases, as no correlation should be given more credit (and more weight) than the one that has the same experimental setup as the simulations conducted. Even if the number of correlations used for averaging was large enough, the averaged result (while being free of experimental deviation) would capture the bias caused by the uneven and more popular experimental settings present in these correlations. If most of the researchers experimented with TR<2, the correlations would be really precise around those TR values but outside this range they would be unreliable, and so would be the average correlation value ($\sum w_i a_{ci} / \sum w_i$).

When compared to the mean correlation's values, simulations have larger discrepancies than when they were compared against Eiamsa-ard et al. (2010)'s correlations. The total average deviation with the mentioned correlations is 28.63% while the total average deviation when compared with the mean correlation value is 29.03%. Total bias found by using the mean correlation value shows that simulations underestimate f by 13% and Nu by 12%, so the accuracy has increased for f and decreased for Nu with respect to the first method. By contrasting simulations in this manner, k-ω models seem to give superior precision than k-ε based models. It is clear that no model can be easily catalogued as the best one for conducting these simulations, as its analysis depends

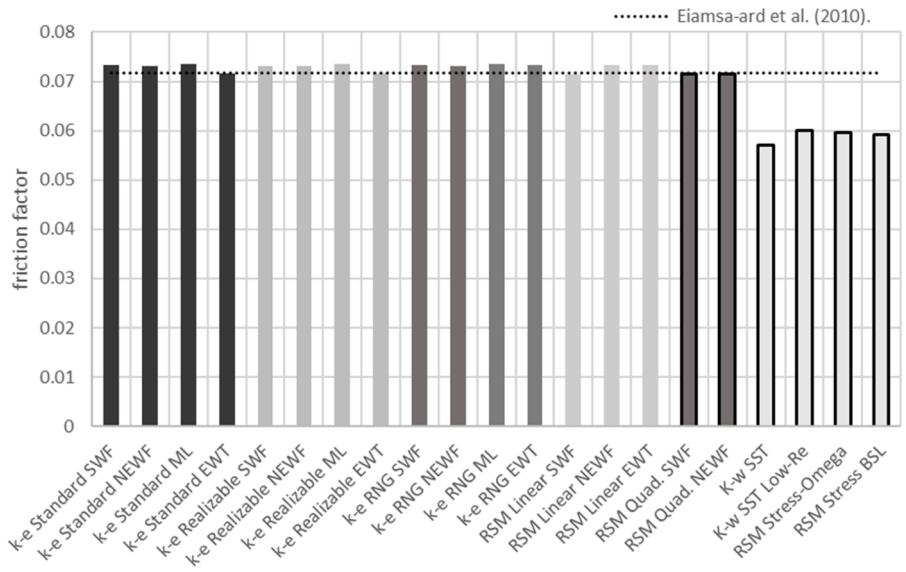

Fig. 14. Friction factor comparison between different models (TR=4, *Re*=10 000).

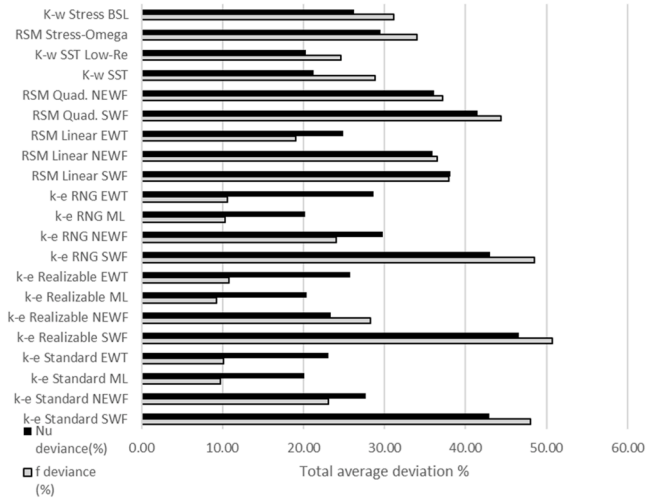

Fig. 15. Total average deviation of each model when compared against correlations in Eiamsa-ard et al. (2010).

on which empirical correlations are considered valid to compare against. These empirical correlations' results differ from each other significantly, so the same result is to be expected when simulations are compared against each other. In fact, simulations do have lower standard deviation between themselves than experimental correlations. While correlations have 44.4% of deviation for f and 16.7% for Nu, simulations grant 24.3% deviation for f and 24.4% for Nu, even though some models are not clearly suited for this case, such as SWF. If the 9 best models are considered, i.e. k-ε models with ML or EWT and k-ω SST models, their deviation is reduced: 17.2% for f and 17.7% for Nu. It is not coincidental that these models and wall treatments agree so much between themselves: ML and EWT are Near Wall $y+$ method that rely on near wall modelling (NWM) when $y+$ is sufficiently small, and with the exception of RSM Stress-Omega (which is used alongside shear flow corrections) all other k-ω based models employ k-ε formulation far from the walls and k-ω's NWM close to the walls. Turbulent models have then proved to be more precise than correlations obtained from experimental data.

Models that use wall functions are clearly outclassed by NWM for such complex geometries. RSM k-ε based models seem to only provide good results when EWT are used (which are only available for RSM Linear Pressure-Strain model), and even in this case they do not seem to give more accurate results than their simpler counterparts. Same is true for RSM k-ω models albeit to a lesser extent: they tend to differ slightly more from correlations than k-ω SST.

Models present different accuracies depending on the geometrical conditions of the simulations, in this case the TR. Lower twist ratios produce more swirling flows and more wall adjacent gradients, which are best modelled by any k-ω model and k-ε based models with ML. These models provide fewer promising results when TR=5, setup in which more shear flow is present in the domain. Models which use EWT are more accurate for higher twist ratios than others, in shear dominated flows, where k-ε based models seem to provide better results, and are precise in all scenarios. This difference might be derived on how different wall treatments extend their boundary layer, based on their own different criteria.

Figs. 15–24 show the contours of velocity and temperature. The contours are taken at the end of the TT, a distance $l = 1.25$ from the inlet. The contours show a point symmetry around the centre of the TT. The fluid is in a counter clockwise swirling motion induced by the TT.

From Figs. 17–19, it is observed that as the flow passes through the twisted tape it accumulates and increases its velocity around the corners that the TT and the outer tube form. More velocity is seen at the top right and bottom left corners, as the flow is being constantly pushed against the wall of the twisted tape at a certain angle, depending on the pitch of the TT. These high velocity zones produce tiny heat boundary layers while slower flow zones are responsible for wider thermal gradients, reflected in the opposite corners of the twisted tape. Fig. 17 shows the different zones of interest: in green fast fluid zones, in blue slow fluid zones and in red, the thermal boundary layer, that becomes thicker in slow velocity zones.

Figs. 18 and 19 show different contours of velocity and temperature for the same case and at the end of the twisted tape, at a distance of 1.25 m from the inlet for k-ε standard and k-ω SST models. Fig. 18 illustrates that different wall treatments calculate differently the thermal layer and the transition layer near the walls. Fig. 18 (a–c) show the results in treatments such as EWT, NEWF or ML and how they capture the swirling flow correctly, having more velocity near the walls of the twisted tape where the flow rotates counter clockwise. ML method exhibits zones of low fluid velocity, which affect negatively the heat transfer, much less present in other methods (Fig. 18b). SWF seem to diffuse the swirling motion of the flow not capturing noticeable gradients in the domain

Table 4
Averaged deviation of the different turbulent models at different twist ratios.

	TR=3		TR=4		TR=5	
	f deviation (%)	Nu deviation (%)	f deviation (%)	Nu deviation (%)	f deviation (%)	Nu deviation (%)
k-ε Standard SWF	26.46	51.63	44.55	43.23	62.83	50.28
k-ε Standard NEWF	12.63	21.28	19.16	28.02	43.56	31.32
k-ε Standard ML	25.78	14.44	3.13	19.34	36.29	17.84
k-ε Standard EWT	50.29	2.87	16.05	17.42	19.13	18.50
k-ε Realizable SWF	29.62	54.43	47.61	46.91	64.98	53.93
k-ε Realizable NEWF	11.07	23.97	25.04	24.28	48.57	26.30
k-ε Realizable ML	26.95	12.72	2.72	19.55	35.99	17.91
k-ε Realizable EWT	51.92	4.02	16.34	19.31	18.54	20.46
k-ε RNG SWF	27.33	52.26	45.10	43.25	63.00	49.76
k-ε RNG NEWF	13.89	23.13	20.48	28.04	45.20	33.06
k-ε RNG ML	24.36	15.00	3.47	19.37	36.52	17.77
k-ε RNG EWT	52.64	7.27	16.01	21.55	19.24	22.49
RSM Linear SWF	29.71	54.76	18.79	15.68	66.07	55.42
RSM Linear NEWF	11.21	24.36	47.66	46.18	50.63	33.48
RSM Linear EWT	57.40	7.40	25.67	28.41	18.39	12.98
RSM Quad. SWF	29.63	54.50	26.44	28.96	66.18	55.71
RSM Quad. NEWF	10.90	24.47	48.20	47.10	51.08	32.99
K-ω SST	8.50	29.72	10.66	3.74	18.78	35.56
K-ω SST Low-*Re*	11.99	5.27	9.99	26.18	19.80	36.20
RSM Stress-Omega	11.19	26.16	8.93	28.95	28.95	37.14
RSM Stress BSL	10.96	26.14	9.05	30.85	26.70	36.47
Average Total	25.45	25.51	22.14	27.92	40.02	33.12

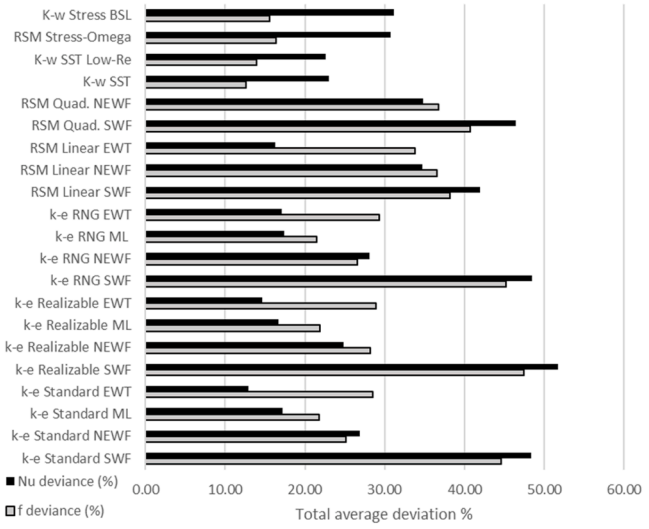

Fig. 16. Total average deviation of each model when compared against mean correlation values.

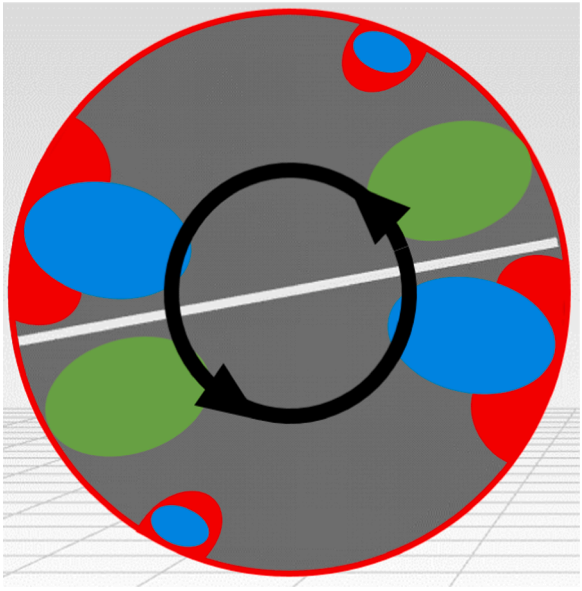

Fig. 17. Graphical guide for the interpretation of physical phenomena depicted.

(Fig. 18d). K-ω SST model displayed in Fig. 18e captures more complex features, and low velocity zones, this time opposite of where ML method predicts them. Although having different profiles, both ML and K-ω SST agree with experimental data in the final pressure drop. But this is not propagated to the heat transfer, where both methods largely disagree on the final heat transferred. In Fig. 19 different shapes and thickness of the thermal layers can be seen, which produce higher or lower Nu numbers.

It is also seen that the slow zones produced in some models caused by the induced swirling generate domains where the thermal boundary layer extends towards the middle of the tube such as the ones seen in Fig. 19(a, b and e), corresponding to EWT, ML and SST. NEWF depicted in Figs. 18 d and 19d show a central low velocity zone that allows the entrance of hot fluid towards the middle of the pipe. From Fig. 19d, corresponding to SWF it can be seen that heat transfer is low, as the temperature near the centre is similar that the inlet temperature. All models exhibit thinner boundary thermal layers in zones where the velocity is higher, where most of the heat is transferred. The main findings that were previously seen in Figs. 18 and 19 are numerically represented and compared in Fig. 20. EWT, NEWF and ML exhibited similar thermal boundary shapes and gradients, providing similar Nu results. Although providing similar friction factor results, both ML and k-ω SST created very different velocity contours, making it difficult to decide which one provided a correct answer.

Deviation's dependency of every model on the Reynolds does not follow clear patterns and in most models the discrepancy with correlations seems to not be affected by Reynolds numbers. There are combinations of models though, that exhibit clear tendencies where the deviation increases or decreases smoothly with the Reynolds number. Nu and f deviation against Eiamsa-ard et al. (2010)'s correlations are averaged along all twist ratios and compared for every Reynolds number. K-ε RNG SWF, RSM Linear and both k-ω SST simulations show increase in friction factor accuracy with higher Reynolds. The opposite is true with K-ε RNG NEWF, who performed better at lower Reynolds. EWT and ML containing models see an increase in Nusselt number accuracy

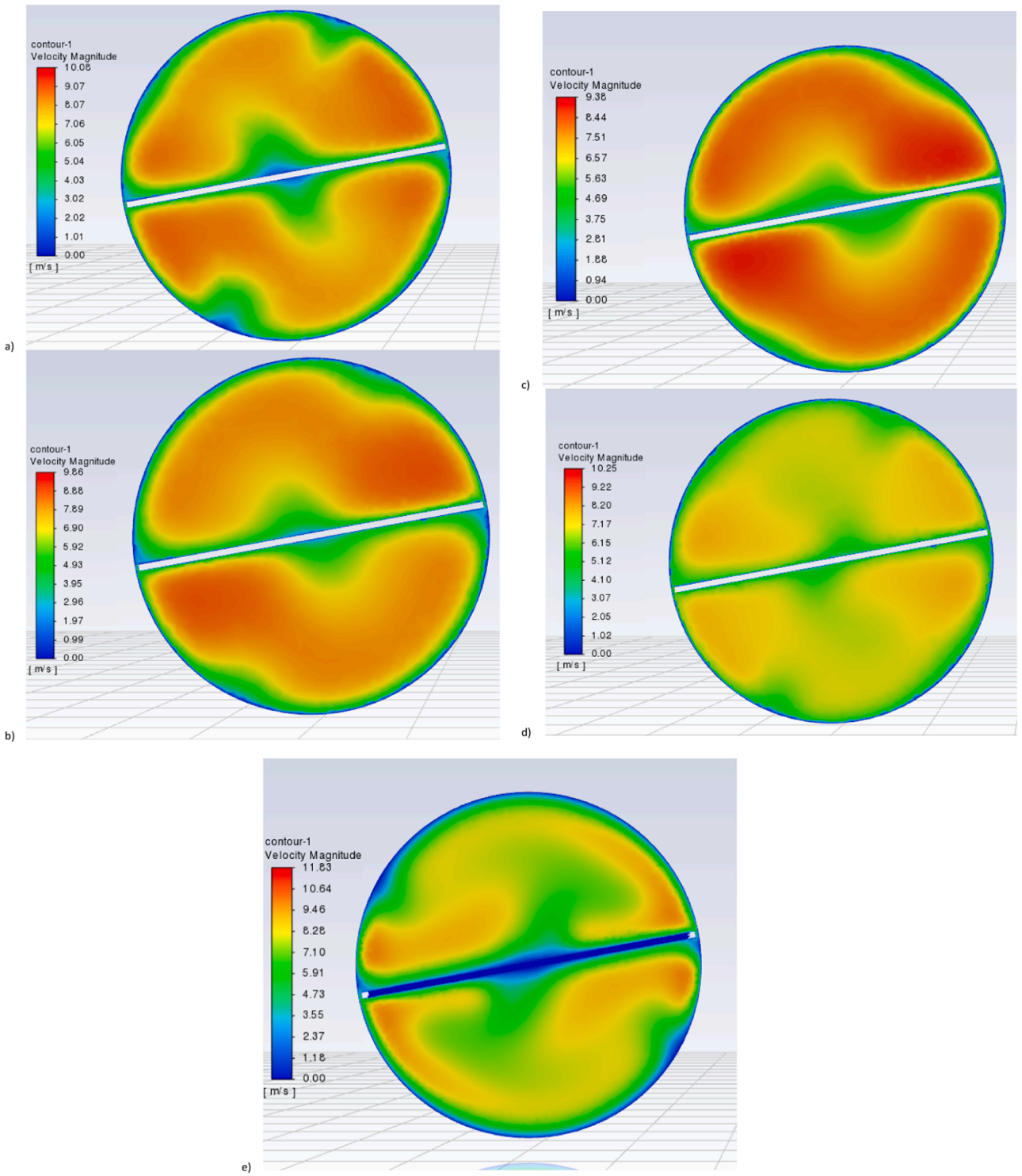

Fig. 18. Velocity magnitude contours, TR=3. *Re*=10 000. Velocity magnitude contours a) K-epsilon St. EWT, b) K-epsilon St. ML, c) K-epsilon St. NEWF d) K-epsilon St.SWF, e) K-omega SST.

with increasing Reynolds while K-ε RNG NEWF and RSM Stress-Omega experienced higher correctness at low Reynolds.

4. Conclusions

Turbulent models prove to be the perfect substitute of experimental correlations, as they have less deviation in their results than them, in addition to providing good agreement with experimental data. If a turbulence deviation present in this research is chosen at random, the expected deviation with experimental correlations when estimating f and Nu is around 29%. Although it is hard to compare results with large collection of experimental correlations that sometimes disagree with each other, some turbulent models and wall treatments can clearly capture the complex features of the flow. When choosing a k-ε models it is of greater importance the wall treatment selected than the k-ε type. The k-ε wall treatments that have provided more accurate results when compared against experimental correlations are EWT and ML, both giving similar results. ML wall treatment is the method that

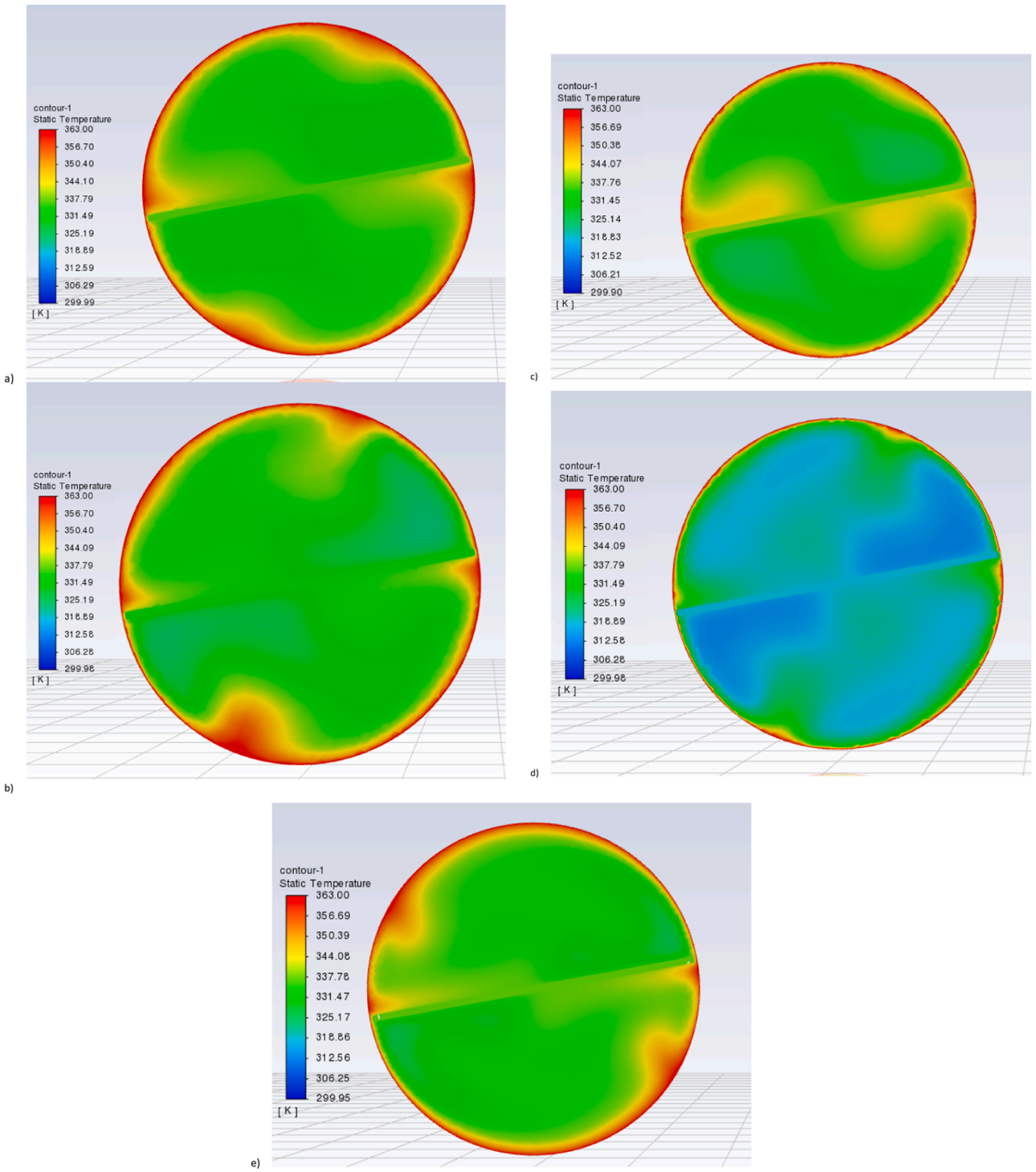

Fig. 19. . Temperature contours:, TR=3. *Re*=10 000. Velocity magnitude contours (a) K-epsilon St. EWT, (b) K-epsilon St. ML, (c) K-epsilon St. NEWF (d) K-epsilon St.SWF, (e) K-omega SST.

comparatively produces less discrepancies with experimental, with an average deviation that ranges from 15% to 18% depending on the comparation method. The SST model is also a solid option with a deviation ranging from 17% to 20%. K-ω models prove to be accurate at predicting pressure loss and capturing important fluid features, especially k-ω SST. While being slightly more accurate in some cases, Low-*Re* corrections did have minor impact on the results. In general, k-ω RSM provide no benefits when conducting these simulations, they seem to be far too complex and require more computational power than two-equation models, also overestimating pressure drop with huge deviations, even when EWT is used along them. K-ω RSM models do not pose any advantage over two-equation k-ω: they provide similar results requiring significantly larger computational time. When different geometrical environments, some models are better suited than others. When *Re* are low and the swirl motion is more relevant ML and k-ω SST models provide more accurate results. K-ω's accuracy diminished at high TR, where shear flows are more dominant. Some model's accuracy increases with the Reynolds number, as it is the case with k-ω SST model, so for $Re>17{,}000$ and $TR\leq 4$, k-ω SST models are advised. Otherwise, in less extreme situations, any k-ε model with ML treatment will provide

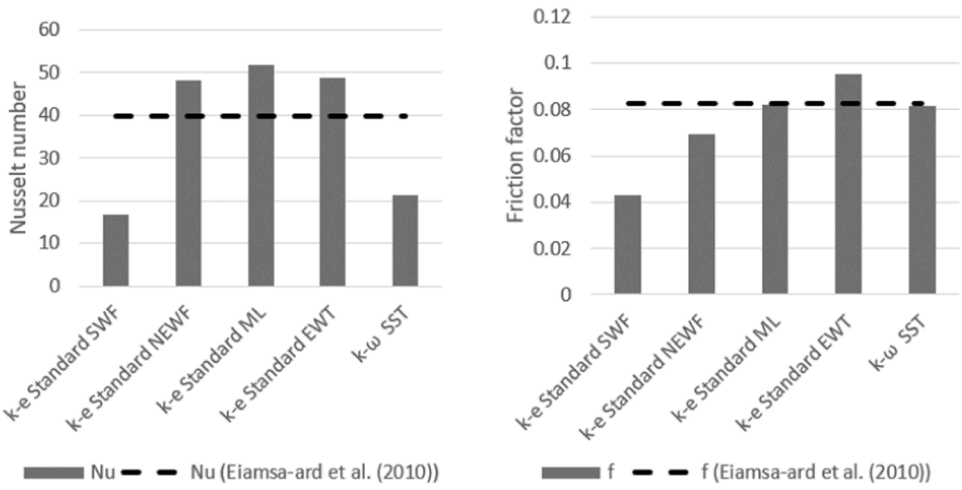

Fig. 20. Deviation with respect to Eiamsa-ard et al. (2010) for the case presented in Figs. 15 and 16.

precise results.

The present study has shown how accurate turbulent models can be at predicting engineering variables, while also delivering keys on how to choose a turbulent model based on the parameters of the problem. Although turbulent models have less deviation than experimental correlations, the choice of a turbulent model and wall treatment can have major impact on the final results so it is of major interest to select adequate models that define properly the flow conditions of the simulated problem.

Declaration of Competing Interest

The authors declare that they have no known competing financial interests or personal relationships that could have appeared to influence the work reported in this paper.

Data availability

No data was used for the research described in the article.

Acknowledgments

The authors would like to thank the financial support of the Fundació Privada Mir Puig who provided the opportunity to complete this research.

References

ANSYS Fluent Theory Guide, 2021. https://ansyshelp.ansys.com/account/secured?returnurl=/Views/Secured/corp/v221/en/flu_th/flu_th_chap_turbulence.html.

Chang, S.W., Jan, Y.J., Liou, J.S., 2007. Turbulent heat transfer and pressure drop in tube fitted with serrated twisted tape. Int. J. Therm. Sci. 46, 506–518. https://doi.org/10.1016/j.ijthermalsci.2006.07.009.

Chu, W.X., Tsai, C.A., Lee, B.H., Cheng, K.Y., Wang, C.C., 2020. Experimental investigation on heat transfer enhancement with twisted tape having various V-cut configurations. Appl. Therm. Eng. 172 https://doi.org/10.1016/j.applthermaleng.2020.115148.

Date, A.W., 1974. Prediction of fully-developed flow in a tube containing a twisted-tape. Int. J. Heat Mass Transf. 17, 845–859. https://doi.org/10.1016/0017-9310(74)90152-5.

Eiamsa-ard, S., Thianpong, C., Eiamsa-ard, P., Promvonge, P., 2010. Thermal characteristics in a heat exchanger tube fitted with dual twisted tape elements in tandem. Int. Commun. Heat Mass Transf. 37, 39–46. https://doi.org/10.1016/j.icheatmasstransfer.2009.08.010.

Eiamsa-ard, S., Thianpong, C., Eiamsa-ard, P., Promvonge, P., 2009. Convective heat transfer in a circular tube with short-length twisted tape insert. Int. Commun. Heat Mass Transf. 36, 365–371. https://doi.org/10.1016/j.icheatmasstransfer.2009.01.006.

Hasanpour, A., Farhadi, M., Sedighi, K., 2016. Experimental heat transfer and pressure drop study on typical, perforated, V-cut and U-cut twisted tapes in a helically corrugated heat exchanger. Int. Commun. Heat Mass Transf. 71, 126–136. https://doi.org/10.1016/j.icheatmasstransfer.2015.12.032.

He, W., Toghraie, D., Lotfipour, A., Pourfattah, F., Karimipour, A., Afrand, M., 2020. Effect of twisted-tape inserts and nanofluid on flow field and heat transfer characteristics in a tube. Int. Commun. Heat Mass Transf. 110 https://doi.org/10.1016/j.icheatmasstransfer.2019.104440.

Hinze, J.O., 1975. Turbulence. McGraw-Hill Publishing Co., New York.

Kumar, A., Prasad, B.N., 2000. Investigation of twisted tape inserted solar water heaters heat transfer, friction factor and thermal performance results. Renew. Energy 19 (3), 379–398. https://doi.org/10.1016/S0960-1481(99)00061-0.

Liao, Q., Xin, M.D., 2000. Augmentation of convective heat transfer inside tubes with three-dimensional internal extended surfaces and twisted-tape inserts. Chem. Eng. J. 78 (2–3), 95–105. https://doi.org/10.1016/S1385-8947(00)00134-0.

Manglik, R.M., Bergles, A.E., 1992. Heat transfer and pressure drop correlations for twisted-tape inserts in isothermal tubes. Part II. Transition and turbulent flows. Am. Soc. Mech. Eng. Heat Transf. Div. 202, 99–106 (Publication) HTD.

Naga Sarada, S., Sita Rama Raju, A.v., Kalyani Radha, K., Syam Sunder, L., 2012. Augmentation of turbulent flow heat transfer in a horizontal tube with varying width twisted tape inserts. Int. J. Automot. Mech. Eng. 6, 797–810. https://doi.org/10.15282/ijame.6.2012.11.0065.

Nakhchi, M.E., Esfahani, J.A., 2020. CFD approach for two-phase CuO nanofluid flow through heat exchangers enhanced by double perforated louvered strip insert. Powder Technol. 367, 877–888. https://doi.org/10.1016/j.powtec.2020.04.043.

Natarajan, A., Venkatesh, R., Gobinath, S., Devakumar, L., Gopalakrishnan, K., 2020. CFD simulation of heat transfer enhancement in circular tube with twisted tape insert by using nanofluids. Mater. Today Proc. 572–577. https://doi.org/10.1016/j.matpr.2019.06.717. Elsevier Ltd.

Noorbakhsh, M., Zaboli, M., Mousavi Ajarostaghi, S.S., 2020. Numerical evaluation of the effect of using twisted tapes as turbulator with various geometries in both sides of a double-pipe heat exchanger. J. Therm. Anal. Calorim. 140, 1341–1353. https://doi.org/10.1007/s10973-019-08509-w.

Oni, T.O., 2021. Analysis of laminar flow and heat transfer characteristics of fluid in plain and induced tubes. Eng. Res. Express 3. https://doi.org/10.1088/2631-8695/abf842.

Oswald, M., 2015. ANSYS Best Practicse Guidelines.

Pourfattah, F., Sabzpooshani, M., Toghraie, D., Asadi, A., 2021. On the optimization of a vertical twisted tape arrangement in a channel subjected to MWCNT–water nanofluid by coupling numerical simulation and genetic algorithm. J. Therm. Anal. Calorim. 144, 189–201. https://doi.org/10.1007/s10973-020-09490-5.

Shabanian, S.R., Rahimi, M., Shahhosseini, M., Alsairafi, A.A., 2011. CFD and experimental studies on heat transfer enhancement in an air cooler equipped with different tube inserts. Int. Commun. Heat Mass Transf. 38, 383–390. https://doi.org/10.1016/j.icheatmasstransfer.2010.12.015.

Sharma, P., Kumar Patel, V., 2020. Computational investigation of the thermo-fluidic effects of inserting twisted tape with alternating twists with notches. Mater. Today Proc. 1968–1972. https://doi.org/10.1016/j.matpr.2020.05.565. Elsevier Ltd.

Tiwari, A.K., Javed, S., Oztop, H.F., Said, Z., Pandya, N.S., 2021. Experimental and numerical investigation on the thermal performance of triple tube heat exchanger equipped with different inserts with WO3/water nanofluid under turbulent condition. Int. J. Therm. Sci. 164 https://doi.org/10.1016/j.ijthermalsci.2021.106861.

Wang, S., Wang, K., Lu, K., Zhang, Q., 2020. Experimental and numerical analysis for thermal-hydraulic characteristics in circular tubes with twisted tape and wire coil inserts. In: Proceedings of the E3S Web of Conferences. EDP Sciences. https://doi.org/10.1051/e3sconf/202016506051.

Zaboli, M., Nourbakhsh, M., Ajarostaghi, S.S.M., 2022. Numerical evaluation of the heat transfer and fluid flow in a corrugated coil tube with lobe-shaped cross-section and two types of spiral twisted tape as swirl generator. J. Therm. Anal. Calorim. 147, 999–1015. https://doi.org/10.1007/s10973-020-10219-7.